BMES BIOMEDICAL ENGINEERING SOCIETY

Check for updates

Original Article

Future Balloon-Expandable Stents: High or Low-Strength Materials?

ALI KHALILIMEYBODI [ORCID],[1] AMIR ALISHZADEH KHOEI,[2] and BABAK SHARIF-KASHANI [ORCID][3]

[1]Department of Biomedical Engineering, University of Virginia, Charlottesville, VA 22908, USA; [2]Department of Mechanical Engineering, College of Engineering, University of Tehran, Tehran, Iran; and [3]Department of Cardiology, Massih-Daneshvari Hospital, Shahid Beheshti University of Medical Sciences, Tehran, Iran

Abstract

Purpose—Recent progress in material science allows researchers to use novel materials with enhanced capabilities like optimum biodegradability, higher strength, and flexibility in the design of coronary stents. Considering the wide range of mechanical properties of existing and newfangled materials, finding the influence of variations in mechanical properties of stent materials is critical for developing a practical design.

Methods—The sensitivity of stent functional characteristics to variations in its material plastic properties is obtained through FEM modeling. Balloon-expandable coronary stent designs: Absorb BVS, and Xience are examined for artificial and commercial polymeric, and metallic materials, respectively. Standard tests including (1) the crimping process followed by stent implantation in an atherosclerotic artery and (2) the three-point bending test, have been simulated according to ASTM standards.

Results—In Absorb BVS, materials with higher yield stress than PLLA have similar residual deflection and maximum bending force to PLLA, which is not the case for Xience stent and Co–Cr. Moreover, elevated yield stress significantly reduces stent flexibility only in Xience stent. For both stents, with different degree of influence, an increase in yield or ultimate stress improves stent radial strength and stiffness and reduces arterial stress and plastic strain of stent, which consequently enhances the stent mechanical performance. Contrarily, yield or ultimate stress elevation increases stent recoil which adversely affects stent performance.

Conclusion—Using high-strength materials has a double-edged sword effect on the stent performance and existing uncertainty in the precise estimate of stent mechanical properties adversely affects the reliability of numerical models' predictions.

Keywords—Finite element analysis, Coronary stents, Material strength, Flexibility, Sensitivity analysis.

Address correspondence to Ali Khalilimeybodi, Department of Biomedical Engineering, University of Virginia, Charlottesville, VA 22908, USA. Electronic mail: ak2jj@virginia.edu

INTRODUCTION

Erstwhile, a few numbers of materials have played the main role in the design of coronary stents and thus there were limited variations in the mechanical properties of stents material. Therefore, researchers have mainly focused their studies on the stent geometric design rather than stent material to enhance the performance of the coronary stents.[5,18,27] But with the advent of the new generation of stents and the use of biodegradable polymers and metals with a wide range of mechanical properties as stent materials, the influence of the material mechanical properties on the stent performance has become particularly important.[2,19,45] Currently, in addition to the permanent coronary stents made of high-strength metal alloys, such as cobalt-chromium alloy, biodegradable stents can be fabricated by a wide variety of biodegradable polymers such as PLLA[22,36] and biocorrodible metal alloys such as magnesium alloys[7,44] based on their chemical composition and bio-absorption time. The wide range of mechanical properties in the new biodegradable materials and changes of their mechanical properties after degradation will lead to large variations in the mechanical performance of future stents. Furthermore, significant variations in the reported or used values of mechanical properties for commercial stent materials like SS316-L, Co–Cr, Mn-based and Fe-based materials in different studies could question the reliability and accuracy of their predictions. Therefore (1) to predict the mechanical performance of future stents with new materials and (2) find the accuracy of the results of existing computational models and (3) estimate the variations of stent functional characteristics due to the gradual loss of mechanical strength in

biodegradable stents during treatment, it is essential to examine the sensitivity of stent functional characteristics to the mechanical properties of its material.

So far, various approaches have been used by researchers to evaluate the mechanical performance of a coronary stent. However, because performing an even small clinical trial on the human coronary arteries can lead to death, using accurate computer simulation is preferred. When we intend to analyze the mechanical performance of a stent, as well as its interaction with the arterial wall, computational models provide a great research tool to complete experimental studies and are sometimes the only possible solution.[15,41] In this regard, Wu et al.[40] investigated the performance of stents fabricated by magnesium alloys for three different designs and showed that the stent design with more mass and optimum mechanical properties can elongate the scaffolding time. In another study, Grogan et al.[11] compared the performance of three stents made of pure iron, magnesium alloy, and stainless steel with the same geometry, based on stent flexibility, radial strength, and recoil. The results indicated that biodegradable stents could compete with modern permanent stents in terms of stent recoil and radial strength. To evaluate the effects of stent material selection, drug coating, and cell design on the mechanical behavior of a metallic stent, Schiavone et al.[30] simulated the deformation of the Xience stent during stenting. They showed that metal stents made of low-strength materials tend to have larger deformations and recoil, but on the other hand, less residual stresses. Schiavone et al. in another study[29] simulated the stenting processes for the Absorb BVS and Xience stents. Their results displayed that the Absorb BVS stent had a lower rate of expansion, higher recoil and lower arterial stress than the Xience stent. Recently, the mechanical performance of PLLA coronary stents has attracted the attention of researchers. On this subject, Pauck and Reddy[23] studied three different PLLA stent designs with a range of Young's modulus to examine the relative effect of stent material stiffness on radial strength, recoil, and radial stiffness of the stent. The authors found highly variable performances for different stent designs. Finally, Wang et al.[39] investigated the mechanical performance of a PLLA stent and determined the stent recoil, flexibility, collapsing pressure, and radial strength and stiffness of the stent.

Although numerous studies have investigated stents performance, only a few studies have looked at the sensitivity of stent functional characteristics to small changes in material mechanical properties. In this study, variations of several stent functional characteristics including stent flexibility, maximum crimping and expanding force, stent recoil after crimping and

expansion, initial and original radial strength and stiffness of stent, arterial wall stress and strain, and residual plastic strain of stent in terms of plastic properties of stent material have been obtained for two commercial stents. We have simulated some standard tests involving stent crimping, expansion of the stent in an artery with symmetrical plaque, and three-point bending test to obtain the functional characteristics of the Absorb BVS and Xience stents as a function of material yield stress and ultimate stress (strain-hardening).

MATERIALS AND METHODS

In this study, two FEM models for the Absorb BVS (Abbot, USA) and Xience (Abbot, USA) stents were developed to study their mechanical performance through Abaqus/Explicit solver. For both stents, different stages of stenting which include (1) Stent crimping, (2) Stent recoil after crimping, (3) Stent expansion in the artery with symmetrical plaque, and (4) Stent recoil after expansion were simulated. The determination of stent flexibility, radial strength and stiffness were also carried out according to the American Society for Testing and Materials (ASTM) standards, *see Online Resource 1*.

Geometric Modeling

The geometric models of Absorb BVS and Xience stents which were created in the SolidWorks software based on their actual images in the expanded state and the reported dimensions in the literature are shown in *Fig. S1 (Online Resource 1)*. For both stents, the initial outer diameter is 3 mm. For complete models, the length of both stents is approximately 18 mm (19 rings for Absorb BVS and 14 rings for Xience), and for partial models (4 adjacent rings), the stent lengths are 3.97 mm and 5.33 mm for Absorb BVS and Xience stents, respectively. Both stents have six peak-to-valley struts in circular direction and strut thickness is 150 μm for Absorb BVS and 81 μm for Xience stent.

In the simulation of stent expansion, researchers used a variety of approaches including: (1) Applying uniform pressure to the inner surface of the stent, (2) Radial displacement on an idealized cylindrical surface and (3) Using the actual balloon model by applying pressure on a tri-folded balloon.[6] Since we do not take into account transient phenomena such as dog-boning and foreshortening and due to the advantages of the second approach like simplicity in the application of boundary conditions, no balloon complexity, and realistic final shape of the expanded stent, the second approach has been selected to reduce

BMES BIOMEDICAL ENGINEERING SOCIETY

computational costs without significantly reducing the accuracy of the results.[10,39,40] So, two idealized cylindrical surfaces with diameter of 4 and 0.5 mm were created in ABAQUS software for stent crimping and expansion, respectively. The length of the cylindrical surfaces is 8 mm, see Fig. 1a.[39]

In previous studies, the atherosclerotic coronary artery was often modeled as an idealized vessel with a localized axisymmetric parabola-shaped stenosis.[15,29,30,40,45] In this study the artery is modeled as a single-layer cylinder with thickness of 1 mm and an axisymmetric plaque layer with a stenosis of 50% is situated in its middle part, see Fig. 1b. The length of artery is 10 mm and the plaque length is selected equal to the length of the examined stent's partial model. In the simulation, a uniform pressure (100 mmHg) is applied to the inner layer of the artery and the plaque before stenting to properly simulate the actual conditions of the arterial wall. Hence, the artery is modeled with primary inner diameter of 2.4 mm, so that after applying the pressure it will increases to about 3 mm.

In this research, the hexahedral linear elements with reduced integration (C3D8R) have been used to discretize stent, artery and plaque solid models.[6,9,10,16,39] The effect of elements size on the simulation results

was analyzed and the results convergence was confirmed based on the stress and strain of the stent and arterial wall, the recoiling effect and radial strength. Also, according to the recommendation of the Abaqus software for C3D8R elements, there are at least four elements in the thickness direction of the stent, artery, and plaque models. The artery, plaque, Absorb BVS stent partial and complete models, and Xience stent partial and complete models were meshed to 13500, 66276, 77980, 130396, 50670 and 102894 elements, respectively. The crimper and expander cylindrical surfaces were also discretized by 1960 and 4898 four-node, shell elements with reduced integration (S4R), respectively (see Fig. 1a).

Material Properties

Stent Material

Coronary stents are generally made of suitable biological materials such as 316L stainless steel or metal alloys and the nature of their behavior is elastic-plastic. In most studies, the stent material has been simplified as a homogeneous and isotropic material, and its behavior is usually defined by bilinear or multilinear
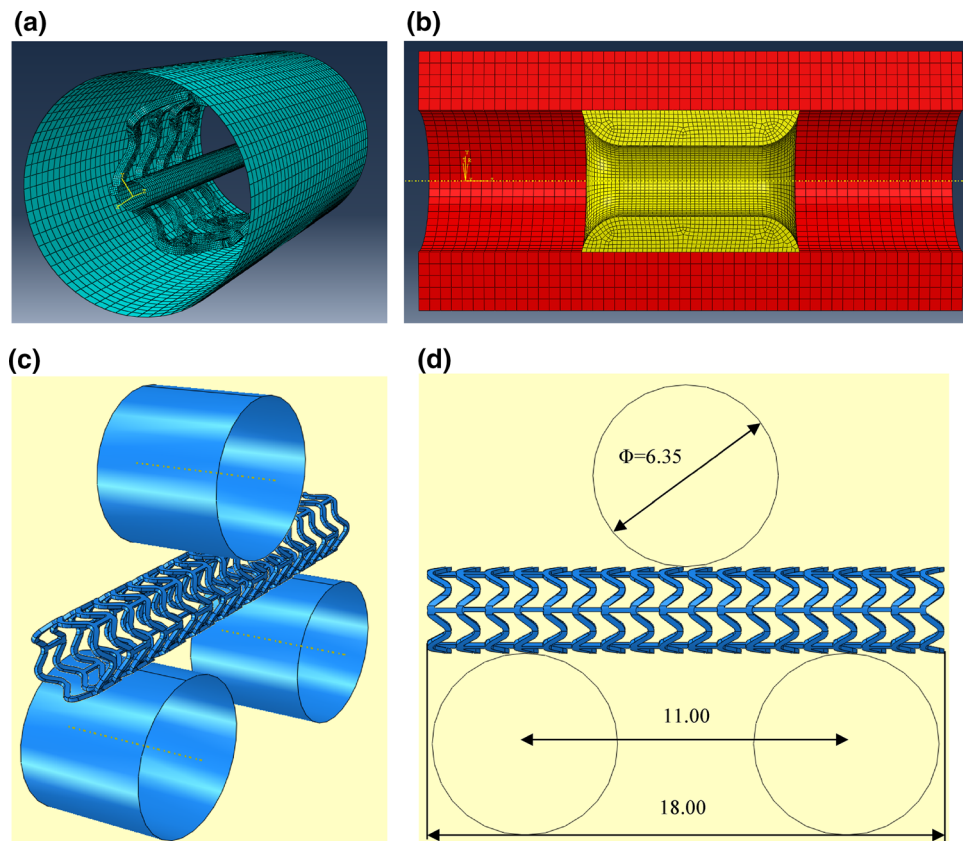

FIGURE 1. The models of (a) expander, crimper, and stent (b) artery and plaque (c, d) three-point bending simulation (unit: mm).

plasticity with isotropic hardening.[18] In this study, the stent material is homogeneous and isotropic, and its non-elastic structural behavior is defined using the von Mises-Hill plasticity model with isotropic hardening in the ABAQUS software. The material stress-strain curve is defined by a bilinear plastic model. The bilinear plastic model without strain-hardening has been used to evaluate the effects of material yield stress on stent functional characteristics. Also, by using a plastic model with linear strain-hardening, several ultimate stresses at 50% plastic strain have been selected to evaluate the effects of material ultimate stress (strain-hardening) on stent functional characteristics.

In order to investigate the sensitivity of the stent functional characteristics to low-strength materials, such as polymers, the Absorb BVS stent and for the high-strength materials such as metallic alloys, the Xience stent was selected. Unlike metallic alloys which manufacturing process and heat treatment mostly determine the variations in their mechanical properties, in the case of polymers, other factors such as molecular weight and temperature also play a major role. So, based on the reported mechanical properties of biocompatible materials in the literature, we created several artificial materials with different yield and ultimate stresses, as shown in Table 1, for the Absorb BVS and Xience stents to investigate the sensitivity of stent mechanical performance to our desired parameters. In the model, Young's modulus for the stent material is 3.3 GPa for the Absorb BVS and 243 GPa for the Xience stent and the Poisson ratio is 0.3 for both stents.[30,39]

Crimper, Expander, Artery and Plaque Materials

In studies that utilize cylindrical surfaces for stent crimping or expansion, the cylinders are often modeled as a rigid surface or a surface with an isotropic elastic material with a very high stiffness (semi-rigid).[11,39,40] Since some researchers applied the latter approach[10,34,39] and verified their numerical results qualitatively and quantitatively, we modeled the crimper and the expander as an elastic shell with an extremely high stiffness (linear elastic modulus of 400 GPa and Poisson ratio of 0.3). It has been shown that in the arterial tissue, prediction of material behavior is difficult due to its nonlinear and anisotropic nature. Hence, in stent studies, it is common to simplify the arterial and plaque material to an incompressible, isotropic, and homogeneous material and define its behavior with a hyperelastic constitutive model. In this study, an isotropic hyperelastic constitutive model with a reduced polynomial strain energy density function of the sixth order (Eq. 1) has been used to model the artery and the plaque.

$$W = C_{10}(I_1 - 3) + C_{20}(I_1 - 3)^2 + C_{30}(I_1 - 3)^3 \\ + C_{40}(I_1 - 3)^4 + C_{50}(I_1 - 3)^5 + C_{60}(I_1 - 3)^6 \quad (1)$$

The coefficients of the arterial strain energy equation were derived from fitting of experimental data for human coronary arteries[12] and for the plaque; they were derived from fitting experimental data of cellular plaque,[17] see Table 2.

Loading Conditions

Determination of Stent Flexibility

In this study, the simulation of the three-point bending test is performed on complete stent model to determine its flexibility.[39] According to the ASTM F2606-08 standard,[32] in the simulation of three-point bending, upper load applicator and lower static supports have been modeled as parallel rigid cylinders with a diameter of 6.35 mm, see Figs. 1c and 1d. For the stent length of 18 mm, the suggested distance between the lower supports is 11 mm and the maximum allowable deformation in the center of stent is 2.2 mm.[32,39] In the simulation of three-point bending test, two stages were defined for controlling displacement of the upper load applicator. In the first step (loading), the load applicator has a downward displacement, which is equivalent to a 1.5 mm deflection in the middle of the stent. The radius of curvature of the stent in this case is 20.9 mm. In the second stage

TABLE 1. Stent material yield and ultimate stresses for studied cases.

Stent	Material property	Case 1	Case 2	Ref.	Case 3	Case 4	Case 5
Absorb BVS	Yield stress	20	40	51.5	60	80	100
Xience		100	300	500	700	1000	1300

Stent	Material property	Ref.	Case 1	Case 2	Case 3	Case 4
Absorb BVS	Ultimate stress	51.5	60	80	100	120
Xience		500	650	800	1000	1200

TABLE 2. Coefficients of the reduced polynomial model for the artery and the plaque in MPa unit.

Material	C_{10}	C_{20}	C_{30}	C_{40}	C_{50}	C_{60}
Artery	6.52e−3	4.89e−2	9.26e−3	0.76	− 0.43	8.69e−2
Plaque	2.38e−3	1.89e−1	− 3.88e−1	3.73	− 2.54	5.73e−1

(unloading), the load applicator exerts back to its original position. The reaction force and displacement of the load applicator are recorded during the simulation and the force-deflection curve is obtained.

Stent Deformation in Crimping

In this section, simulation of the stent crimping process from the initial outer diameter to the appropriate diameter for the placement on the catheter is performed to examine the initial radial strength and stiffness of the stent and the stent recoil after crimping. First, by using the radial shrink of the crimper, the stent is crimped to an outer diameter of 1.3 mm, and second, the crimper diameter gradually returns to its original value during stent spring-back. The stent crimping process is designed such that the final outer diameter of the stent after recoil is about 1.5 mm which fits inside the atherosclerotic artery.[29]

Stent Deformation in Confined Expansion

In this section, the expansion of the stent from its compressed state (released after crimping) to its expanded state in the atherosclerotic artery is simulated to examine the stent expandability and its recoil after expansion. In this simulation, the loading process involves two steps. In the first step, without considering the expander and the stent, an internal constant pressure of 100 mmHg (13.3 kPa) is applied on the inner surfaces of the artery and plaque.[10,14,15] In the second step, by holding the pressure constant, the expansion of the stent is achieved by radial expansion of the expander to diameter of 3.1 mm (inflation) and then the expander returns to its initial diameter (deflation).

Determination of Radial Strength and Stiffness

The determination of stent radial strength and stiffness occurs while the stent is in its operational diameter after stenting. So, in the following of stent recoil after expansion inside the artery, the outer diameter of the stent decreases 0.8 mm by the crimper, and then, during the stent spring-back, the crimper gradually returns to its original diameter. The contact force and outer diameter of the stent are recorded during the process and its radial loading curve is generated. Afterwards, according to ASTM F3067-14 standard,[33] the radial strength and stiffness of the studied stent are obtained.[39]

Boundary Conditions

In order to simulate the stenting process, the stent should be able to expand and compress in the radial and longitudinal directions, while it should have been fixed somehow to have no rigid body motion. In this study, similar to Gervaso *et al.* study,[10] we limited the tangential and longitudinal movements of 3 nodes on the middle plane of the stent, and the artery which form the corners of an equilateral triangle. The interface between the arterial wall and the plaque was assumed to be coherent. The interaction between stent and atherosclerotic artery and between stent, and crimper or expander surfaces were considered as surface to surface hard contacts with penalty formulation and a friction coefficient of 0.25.[29,30] The interaction between stent, supports and load applicator in three-point bending were assumed to be surface to surface contact with a friction coefficient of 0.15. Also, the frictionless self-contact has been defined for stent rings.[39]

Solution Methodology

In this study, due to the large deformation of the stent, artery and plaque, as well as the complexity of contacts between the different surfaces, the Abaqus/explicit solver has been used to perform the analysis. Also, an automatic stabilizer has been used in simulation to achieve the convergence of contact. At each step, based on the Abaqus recommendation, the kinetic energy of the whole model was compared with the internal energy and the simulation time (loading rate) was selected in such a way that, in all simulation steps, the ratio was less than 5% in order to satisfy the quasi-static conditions.[6,11,30] The automatic time increment was used for the simulation and it was on the order of 10^{-8}.

RESULTS AND DISCUSSION

Determination of Stent Flexibility

In this section, the simulation results of the three-point bending test for the Absorb BVS and Xience stents are presented. Figures 2a and 2b show the elastic-plastic deformation and von Mises stress distribution of Absorb BVS and Xience stents in the
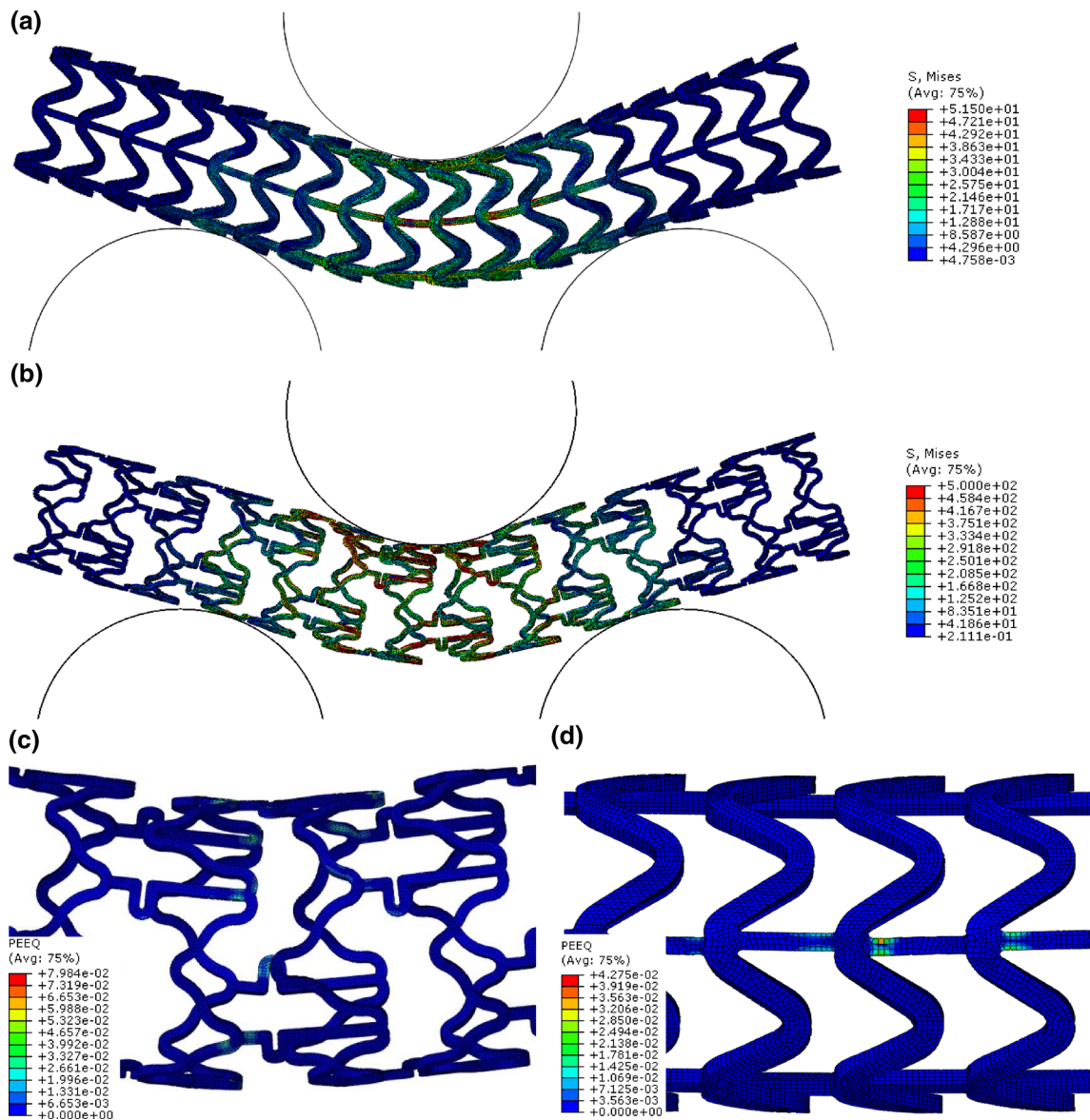
FIGURE 2. Simulated results of three-point bending test. Simulated profile and von Mises stress distribution of (a) Absorb BVS and (b) Xience stents at maximum deflection. The residual equivalent plastic distribution of (c) Absorb BVS and (d) Xience stent after unloading in three-point bending test.

maximum deflection for reference materials, respectively. As seen from Figs. 2c and 2d, the highest equivalent plastic strain occurs at the middle of the stent and often in the bridges connection to the stent rings.[39]

The variations of stent functional characteristics in terms of material yield stress for Absorb BVS and Xience stents in three-point bending test are presented in Table S1 (Online Resource 1). *For definition of these functional characteristics, please refer to the Online Resource 1.* As can be seen from Table S1, for the Absorb BVS stent, with the increase in yield stress, the onset of the material plastic deformation is postponed, so that in cases with high yield stress, there is no plastic

deformation at all. Also, the higher yield stress leads to the less zero force deflection. For the yield stresses above 50 MPa, there are no residual stent deflections after unloading. Moreover, increase in yield stress results in the higher ratio of material elastic to plastic deformation and decreases the force hysteresis. The variations of the stent functional characteristics in terms of yield stress for the Xience stent are like the Absorb BVS stent. But, due to the higher Young's modulus and yield stress in metal alloys than polymers, the maximum bending force and force hysteresis are in Xience stent are higher than Absorb BVS. Regarding the reported functional variables, except for the maximum bending force, it can be concluded that increased

BMES BIOMEDICAL ENGINEERING SOCIETY

yield stress improves stent mechanical performance. However, since the maximum bending force variable directly correlated with bending stiffness, the increase in the yield stress has an adverse effect on the stent flexibility. The more bending stiffness, the less stent flexibility.

Table S2 (Online Resource 1) shows the variations in stent functional characteristics in terms of material ultimate stress in Absorb BVS and Xience stents. As shown in Table S2 for the Absorb BVS stent, the values of deflection at initial plastic flow, residual deflection and maximum bending force variables are same for different ultimate stresses. However, with the increase in ultimate stress (or strain hardening), the plastic deformation of the Absorb BVS stent decreases slightly, which is apparent from the decreasing trend of zero force deflection and the force hysteresis with increasing ultimate stress. In the Xience stent, the deflection at initial plastic flow is same for all cases except for the reference material. Also, increase in the ultimate stress results in the reduction of zero force deflection, residual stent deflection and elevation of maximum bending force and no change in the force hysteresis. Nevertheless, it is observed that the sensitivity of the stent functional characteristics to changes in the ultimate stress is far less than to changes in the yield stress which is due to the high ratio of elastic to plastic deformation of stent in the three-point bending test. Therefore, we can conclude that changes in the ultimate stress (or strain hardening) have a little effect on stent flexibility.

The main results of three-point bending test including the variation of bending stiffness and maximum of residual equivalent plastic strain in terms of yield and ultimate stress for the Absorb BVS and Xience stents are presented in Fig. 3. As can be seen, we observe significant variations in the bending stiffness only for the Xience stent in terms of yield stress (Fig. 3a) and other cases are not significant. In general, The Xience stent has higher bending stiffness than Absorb BVS (Figs. 3a, 3b). Also, increase in the yield or ultimate stress reduces the maximum of residual equivalent plastic strain in both stents. As can be seen from Figs. 3c and 3d, the effect of variations in the yield stress on residual plastic strain is much higher than the ultimate stress.

Stent Deformation in Crimping

In this section, to evaluate the effects of material plastic properties on the function of the stent during compression, the functional variables including the initial radial strength, the initial radial stiffness, the maximum force for the stent crimping, the stent recoil after crimping, and the equivalent plastic strain after recoil have been determined for the Absorb BVS and Xience stents with different plastic properties. *The definitions and methods to obtain these functional characteristics are described in the Online Resource 1.* In addition to the radial strength and stiffness of the stent which are obtained in the re-compression stage after the stent expansion, we calculated the initial radial strength and stiffness of the stent from the radial loading curves at the crimping stage. Figures 4a–4d show the deformation and the von Mises stress distribution in the Absorb BVS and Xience stents for the reference materials in the fully crimped configuration and after spring-back. As shown in Figs. 4a and 4b, the maximum von Mises stress for both stents are at both sides of the U-bends. The von Mises stresses at the U-bends are equal to stent material yield stress in the fully crimped configuration and reduce nearly 40% after the stent spring-back.

The changes in the stent functional characteristics related to the crimping stage in terms of the material yield stress are presented in Table S3 (Online Resource 1). According to the results, increase in the material yield stress in both stents results in the roughly linear decrease of the residual equivalent plastic strain and the roughly linear increase of the maximum crimping force, and the initial radial strength of the stent. As shown in Fig. 4e, higher yield stress results in more crimping recoil for both stents in a linear way. Also, the initial radial stiffness is increased nonlinearly for both stents. However, the initial radial stiffness of the Absorb BVS stent is approximately constant for yield stresses above 60 MPa. In general, according to the results, it can be concluded that the increase in the yield stress has a dual effect on the mechanical performance of the stent in the crimping stage. In one hand, it improves the mechanical performance of the stent based on the changes in the residual plastic strain, radial strength and radial stiffness of the stent, and on the other hand, in terms of the maximum crimping force and the stent recoil after crimping, has an adverse effect on stent performance.

Table S4 (Online Resource 1) presents the variations of the stent functional variables for the crimping stage in terms of the material ultimate stress. The results indicate that in the Absorb BVS stent, with the increase in ultimate stress, the residual equivalent plastic strain is reduced nonlinearly. This event is due to the increase in the material strain-hardening and, consequently, reduction of the material plastic deformation. Also, variations of the maximum crimping force in respond to the increase in ultimate stress is like its response to elevation of yield stress, but with less sensitivity. Furthermore, increase in the ultimate stress results in a linear elevation of the initial radial strength and stiffness of the Absorb BVS stent. But this eleva-
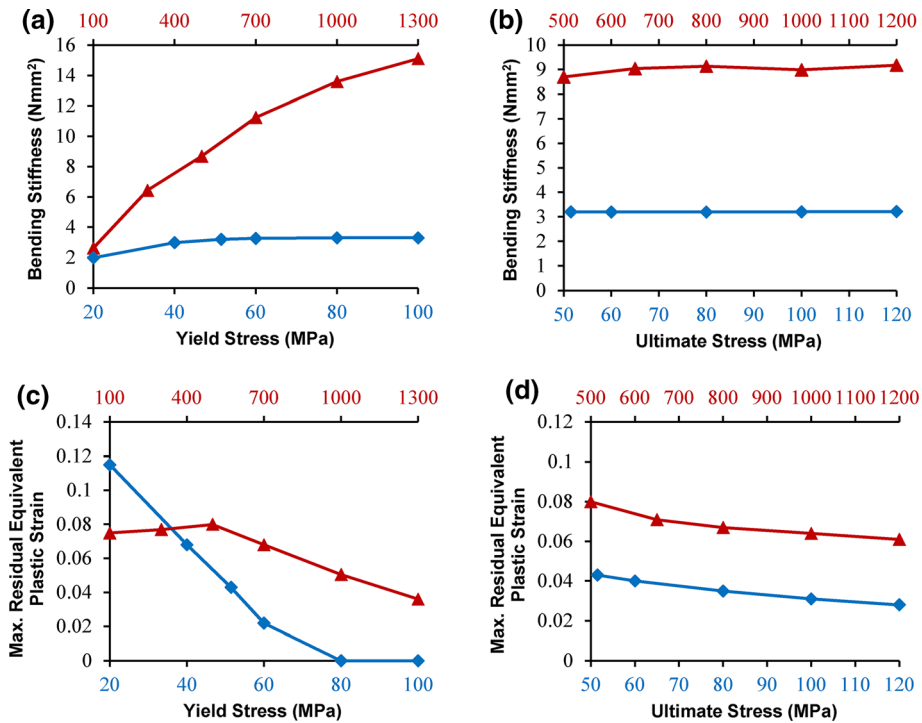
FIGURE 3. Three-point bending test results. (a, b) Variations of bending stiffness and (c, d) maximum of residual equivalent plastic strain in the Absorb BVS (filled diamond) and Xience (filled triangle) stents in terms of material (a, c) yield stress and (b, d) ultimate stress.
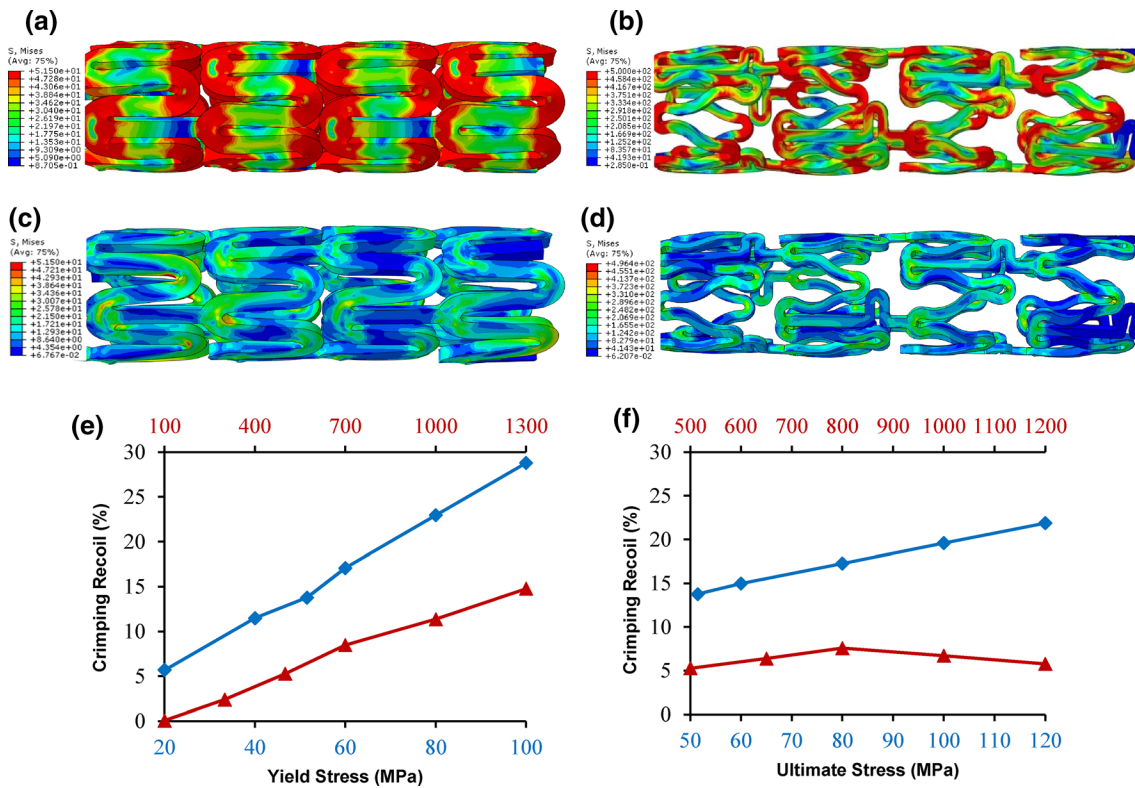

FIGURE 4. Simulation results of stent crimping. Distribution of von Mises stress on the Absorb BVS and Xience stents in (a, b) fully crimped and (c, d) after spring-back states, respectively. Variations of stent crimping recoil in terms of material (e) yield stress and (f) ultimate stress in the Absorb BVS (filled diamond) and Xience (filled triangle) stents.

tion is only valid for ultimate stresses up to 100 MPa and both characteristics remain constant for ultimate stresses above that. However, the initial radial stiffness changes in terms of ultimate stress are negligible. As shown in Fig. 4f, higher ultimate stress results in more crimping recoil for Absorb BVS stent in a linear way. But, its effect on Xience stent is nonmonotonic and the maximum crimping recoil happens in moderate ultimate stress which implies on more nonlinear response in Xience stent. In general, it can be concluded that the increase in ultimate stress has the same dual effects as increasing the yield stress on the mechanical performance of the Absorb BVS stent in the crimping stage, but these effects are much less.

The variations of the residual equivalent plastic strain, the maximum crimping force, initial radial strength and stiffness in terms of the ultimate stress in the Xience stent are like the Absorb BVS stent. But,

unlike the Absorb BVS stent, the Xience stent with the ultimate stress of 800 MPa has the maximum stent recoil after crimping. Finally, it can be concluded that the increase in the material ultimate stress has a positive effect on the mechanical performance of the Xience stent.

Stent Deformation in Confined Expansion

In this section, the expansion of the Absorb BVS and Xience stents in an artery with a symmetrical plaque are simulated and the results are presented as changes of the stent functional variables in terms of the plastic properties of the stent material. The both stents have been expanded to inner diameter of 3.1 mm until the final inner diameter of both stent after their recoil come close to the inner diameter of the artery (3 mm). Figures 5a and 5b illustrate the expanded state of the
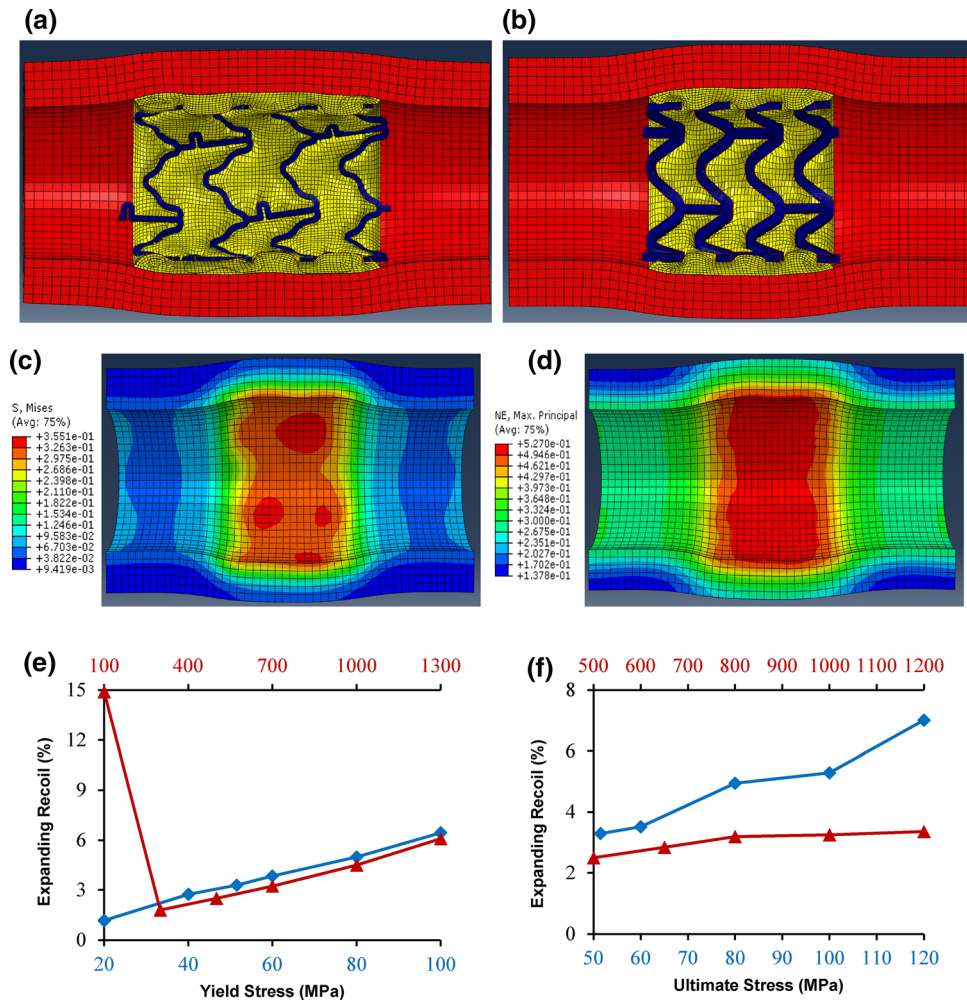

FIGURE 5. Simulation results of stent confined expansion. Artery and plaque deformation in the expansion of (a) Xience and (b) Absorb BVS stents. Distribution of (c) von Mises stress and (d) maximum principal strain in the arterial wall after implantation Absorb BVS stent. Variations of stent expanding recoil in terms of material (e) yield stress and (f) ultimate stress in the Absorb BVS (filled diamond) and Xience (filled triangle) stents.

Xience and Absorb stents in the artery after their expanding recoil. The stent functional variables in this section include stent recoil after expansion, maximum expansion force and the residual equivalent plastic strain. *For definition of stent recoil after expansion, please refer to the Online Resource 1.* In addition to the described functional variables, the artery stress and strain also play a major role in the stent performance and it has been shown that their excessive increase leads to the damage to the artery and undesirable cell proliferation and consequently reduces the effective performance of the stent. Figures 5c and 5d show the distribution of von Mises stress and maximum principal strain of the artery wall after stent expanding recoil for the Absorb BVS stent.

Table S5 (Online Resource 1) presents the changes of stent functional variables related to the expansion stage in terms of the material yield stress. In both stents, by increasing yield stress, the residual equivalent plastic strain reduces linearly. On the other hand, increase in the yield stress results in the linear elevation of the maximum expansion force. As shown in Fig. 5e, increase in the yield stress linearly elevates stent recoil for both stents. However, in the Xience stent, unlike the general trend of stent recoil, the expanding recoil is very high in the yield stress of 100 MPa. The very low strength of the Xience stent in this case results in the domination of the reversal force of artery and plaque on the stent and eventually increases the stent recoil. Also, only in this case, the stent lost its cylindrical shape after unloading and was bent in the shape of the plaque.

Furthermore, the materials with the yield stress of 40 MPa in the Absorb BVS and 300 MPa in the Xience stent have the highest value of the arterial wall strain and stress. However, changes in the arterial wall strain and stress for the different yield stresses are little in both stents. In general, according to the variations of all functional characteristics, the increase in the yield stress has a dual effect on stent performance in confined expansion. On one hand, it reduces the plastic strain of the stent and the arterial wall strain and stress which improve the performance of the stent, and on the other hand, it increases the force (pressure) required for the stent expansion and the expanding recoil of the stent which diminish the stent efficiency.

The changes of the functional variables of the expansion stage in terms of the material ultimate stress are shown in Table S6 (Online Resource 1). As the material ultimate stress increases, the amount of residual equivalent strain is reduced nonlinearly in both stents. The results also indicate a linear increase in the maximum expansion force in both stents with increasing ultimate stress. As shown in Fig. 5f, an increase in the ultimate stress results in a nonlinear increase in the stent recoil after expansion for the Absorb BVS stent. The expanding recoil in the Xience stent remains nearly constant with the increase in the ultimate stress. Moreover, with increasing material ultimate stress, we see a linear decline in the stress and strain of the artery in both stents. Overall, it is observed that the increase in ultimate stress has a dual effect on the performance of the Absorb BVS and Xience stent, but seems its positive effect is more prevalent on the Xience stents.

Determination of Radial Strength and Stiffness

Because of the role of the residual stress and strain of stent on its radial performance, we determined the radial strength and stiffness of the stent in a re-crimping stage that is performed after stent expansion in the artery. The variations of the radial strength, radial stiffness and zero compression diameter in terms of yield stress are presented for both stents in Table 3.

In both stents, with increasing yield stress, the radial strength and stiffness increase significantly and zero compression diameter decreases. But, in the Xience stent, we have an exception for the zero-compression diameter in the yield stress of 100 MPa that is due to the extremely low strength of the Xience stent in this case. The results in Table 4 indicates the variations of the radial strength, radial stiffness and zero compression diameter in terms of ultimate stress. In the both stents, with increasing ultimate stress, the radial strength and stiffness increase and the zero compression diameter decreases. In general, increase in the yield or ultimate stress has positive effects on the

TABLE 3. The variations of stent radial strength and stiffness and zero compression diameter in terms of material yield stress.

Stent	Material Property	Case 1	Case 2	Ref.	Case 3	Case 4	Case 5
Absorb BVS	Radial strength (N/mm)	0.38	0.86	1.15	1.29	1.68	1.953
	Radial stiffness (kPa/mm)	189	447	592	621	702	749
	Zero compression diameter (mm)	3.314	3.295	3.251	3.236	3.179	3.128
Xience	Radial strength (N/mm)	0.25	0.54	0.90	1.43	2.24	2.82
	Radial stiffness (kPa/mm)	82	634	1046	1556	1734	1932
	Zero compression diameter (mm)	3.098	3.293	3.281	3.233	3.197	3.151

BMES BIOMEDICAL ENGINEERING SOCIETY

TABLE 4. The variations of stent radial strength and stiffness and zero compression diameter in terms of material ultimate stress.

Stent	Material Property	Ref.	Case 1	Case 2	Case 3	Case 4
Absorb BVS	Radial strength (N/mm)	1.15	1.29	1.76	2.05	2.41
	Radial stiffness (kPa/mm)	592.3	654.8	711.3	850	865.6
	Zero compression diameter (mm)	3.251	3.236	3.202	3.174	3.132
Xience	Radial strength (N/mm)	0.90	1.40	1.61	1.75	1.93
	Radial stiffness (kPa/mm)	1046	1003	1068	1110	1250
	Zero compression diameter (mm)	3.281	3.265	3.252	3.243	3.179

stent's ability to keep the artery open. Moreover, by comparing the radial strength and stiffness of both stent in different cases with their initial values that has been reported in section 3.2, it is found that stenting process diminishes the radial strength and stiffness of stent.

The Influence of Inaccuracy in Material Mechanical Properties on Model Predictions

Since the invent of coronary stents, numerical methods play an impartible part of stent design. But, apart from the inherent errors in these methods, any inaccuracy in defining the material could result in excessive errors. Although there are limited biocompatible materials that currently have been used commercially for manufacturing stents, the exact value of the material mechanical properties for each specific stent is often unknown. For example, CoCrL605, SS316L, and PLLA are the known stent materials, but there are quite wide ranges of reported or used values for their mechanical properties (Fig. 6). Most of these variations are due to the difference in the material treatments like heat treatment, manufacturing process, the chemical compositions, and the measurement methods and devices. But, the source of error doesn't change this fact that there are many numerical studies with the same stent and material, but different mechanical properties.

So, in order to evaluate the effects of inaccuracy in material mechanical properties on the numerical model predictions, we obtained the reported or used values of stent materials yield and ultimate stresses for the known metallic (Fig. 6a) and polymeric stent materials (Fig. 6d) and then simulated the three-point bending and stent confined expansion for the Xience and Absorb BVS stents with the selected materials. As shown in Figs. 6b and 6c for the Xience stent and metallic materials, materials with higher yield and ultimate stress generally result in a higher radial strength, bending stiffness (lower flexibility), and stent recoil. But there are some exceptions like higher stent recoil for low-strength materials such as Mg-based alloys or pure Fe that is due to the lower elasticity module of

these materials which increases stent recoil. By comparing the materials with similar elasticity module (same color in Figs. 6b and 6c), the results with existing stent materials are like the results of simulation with artificial materials in previous sections. The same results can be obtained for the polymeric materials and Absorb BVS stent as shown by Figs. 6e and 6f.

For example, as shown in Fig. 6a, the yield and ultimate stress of CoCr[L605] (Xience stent base material) from Ref. 37 are 34 and 15% higher than Ref. 25 respectively, which results in the 20% increase in bending stiffness, 37% increase in stent recoil and 15% increase in stent radial strength. These results show that variations in material plastic properties have a significant effect on the stent functional characteristics and highlight the importance of obtaining the exact mechanical properties of stent material for numerical studies.

Finding an Optimum Yield and Ultimate Stress

In general, finding an optimum stent design is highly dependent on the design goals. Since changing the stent geometry is much easier than changing its material, many designers prefer to reach optimal stent functional characteristics by optimizing stent geometrical design with a fixed material. But as shown in Figs. 6a and 6d, assuming a material with fixed mechanical properties is not always reasonable. Moreover, for biodegradable stents, a decrease in the stent material mechanical strength during the time complicates the process of finding an optimum geometry. Therefore, optimizing the material for a fixed geometry could be a sensible solution in some cases.

Based on the results of previous sections for Xience stent, using materials with higher yield stress in one hand increases stent radial strength and stiffness and reduces arterial stress and plastic strain of stent which improve stent function in the artery. On the other hand, higher yield stress decreases stent flexibility (higher bending stiffness) and increases stent recoil which decreases the stent performance. Based on Fig. 5e and assuming the acceptable stent recoil should be lower than 4%, the maximum acceptable yield
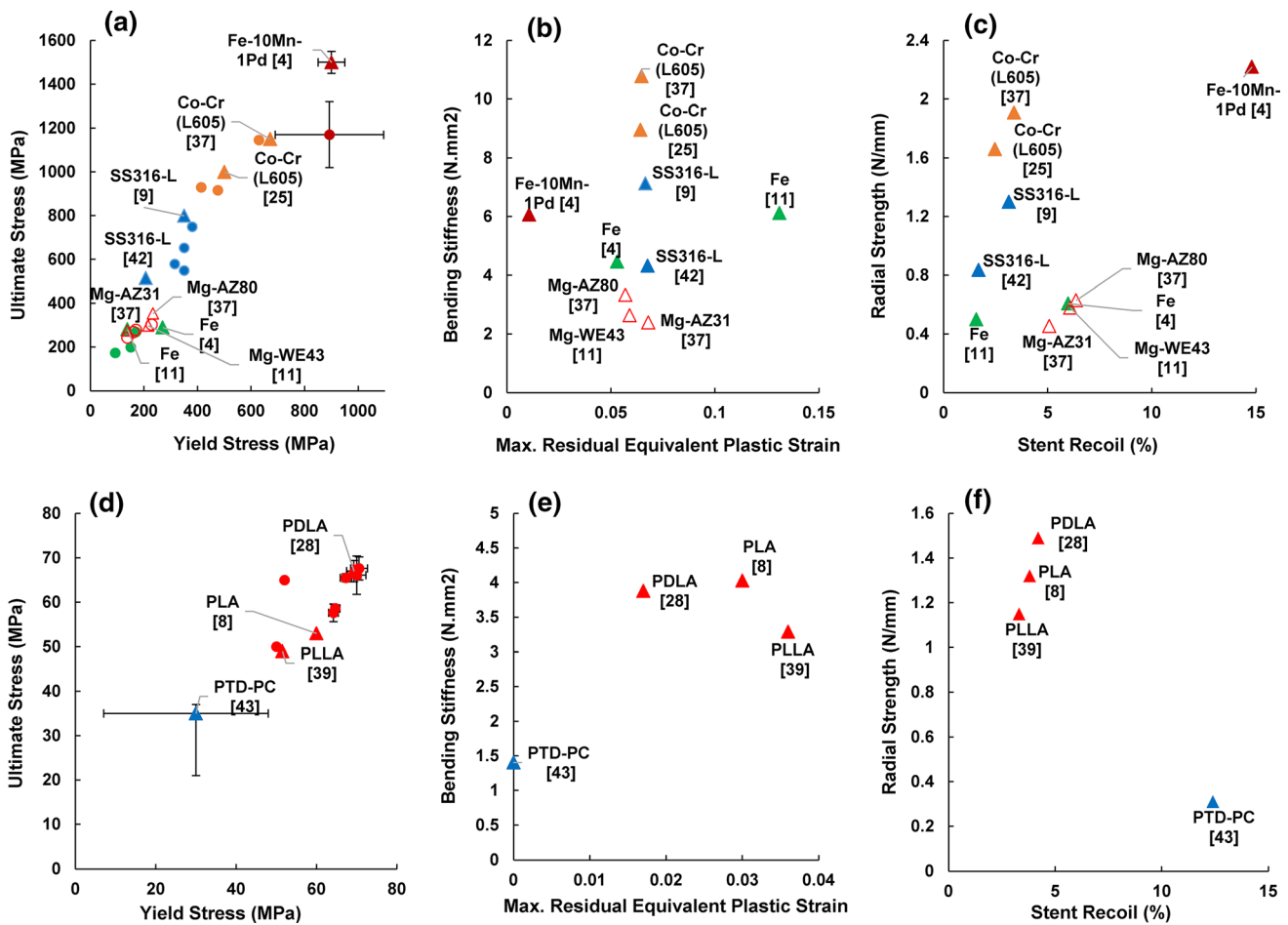
FIGURE 6. The influence of variations in plastic properties of metallic and polymeric stent materials on stent functional characteristics for Xience and Absorb BVS design. (a) Yield and ultimate stresses of several metallic biocompatible materials including different grades of CoCr (filled orange[11,13,20,25,37]), SS316L (filled blue[1,9,11,16,37,42]), Fe alloys (filled crimson red[4]), pure Fe (filled green[4,11,21]), and Mg-based (non-filled red[4,11,37]) alloys. The triangles shows the materials that are selected for simulation. (b) Variations of bending stiffness and maximum of residual equivalent plastic strain in three-point bending test and (c) radial strength and stent expanding recoil in confined expansion for selected metallic materials with Xience stent. (d) Yield and ultimate stresses of several polymeric biocompatible materials[8,28,39,43] (e) Variations of bending stiffness and maximum of residual equivalent plastic strain in three-point bending test and (f) radial strength and stent expanding recoil in confined expansion for selected polymeric materials with Absorb BVS stent. In all subfigures, same color means similar elasticity module and density.

strength is 880 MPa which yields to the 12.6 N mm^2 bending stiffness (Fig. 3a). because the variations of ultimate stress have not any significant effect on the stent recoil (Fig. 5f) and bending stiffness (Fig. 3b) but slightly improves other factors, a material with yield stress lower than 880 and the highest ultimate stress is suitable for Xience design. Also, because the relation between bending stiffness and yield stress is nonlinear for this range of yield stress (Fig. 3a), lower yield stress significantly reduces bending stiffness and improves stent performance. Therefore, among the materials that are illustrated in Fig. 6a, Co–Cr[L605] with yield and ultimate stress equal to 670 and 1150 MPa, respectively, is the best choice. The Fe alloys (crimson red) are near the threshold too, but due to the lower

elasticity module in these materials, their recoil is very high and not acceptable.

Since the overall response of Absorb BVS stent to variations in yield and ultimate stress is like Xience stent, we use the same approach. Based on Fig. 3a, an increase in yield stress does not elevate bending stiffness significantly, so the main problem in using higher strength material is stent recoil. Considering the 4% threshold for the maximum stent recoil, according to Fig. 5e, material yield stress should be lower than 62 MPa. An increase in ultimate stress has not any effect on bending stiffness of Absorb BVS design (Fig. 3b) and according to Fig. 5f the ultimate stress should be lower than 67 MPa. Among the polymeric materials in Fig. 6d, PLA with yield and ultimate stress equal to 60

and 53 MPa is the best choice. It is noteworthy that this optimization process was based only on the stent mechanical performance in the artery and finding an optimum material needs considering other biological factors and the amount of decrease in the material strength during treatment for biodegradable stents, which is out of the scope of this study.

Comparison and Verification of the Results

In a study on a PLLA stent by Wang *et al.*[39] that is similar to our Absorb BVS stent model with reference material in terms of geometry and material, the authors observed that the maximum deformation of the stent during crimping process mostly take places at the inner surfaces of peak and valley bows and the maximum equivalent plastic strain is 0.214 for outer diameters of 2.6 mm and 0.793 for outer diameters of 1.8 mm. In this study, we obtained similar simulation results with the maximum equivalent plastic strain of 0.231 and 0.789 in the outer diameters of 2.6 and 1.8 mm, respectively, for the Absorb BVS stent during crimping process.

Also, Wang *et al.*[39] observed a phenomenon called crazing at the peaks and valleys of the stent during the crimping process which is due to the accumulation and increase of the plastic strain in those points. Moreover, they observed that the *in vitro* deformation of the stent strut during crimping was approximately symmetrical down to 2.6 mm in diameter and then it was asymmetrical. As shown in Fig. 7, the simulation results of the present study predict well the experimental results of Wang *et al.* study[39] in terms of stent's deformation type and occurrence of the crazing in the peak and the valley of the stent during crimping process.

As shown in Fig. 8a, the stent recoil after crimping and expansion for the Absorb BVS stent model with the reference material is compared with the numerical and experimental result of previous studies. The stent recoil after expansion, in addition to the stent material, largely depends on the material properties of the plaque and the artery. For instance, cellular, hypocellular, and calcified plaques with different degrees of calcification result in different stent recoils after expansion.[24] In an experimental study, Borghi *et al.*[3] obtained the acute recoil of the Absorb BVS stent after expansion in 25 different patients, varying between 2.6 and 11.6%. In another study, Qiu *et al.*[26] showed that the loading rate also influences the stent recoil after expansion and with increasing loading rate, the stent recoil decreases. Therefore, in addition to the stent material, other factors such as patient conditions, the degree of stenosis, loading conditions, and the artery and the plaque material properties contribute in the stent behavior and its recoil. However, the calculated stent recoil after expansion for the Absorb BVS stent model is 3.3 for reference material and it is close to the reported value in the manufacturer document,[35] 3.7 mm, and it is also in the range of experimental results, see Fig. 8a.

We also compared our results for the Absorb BVS stent with numerical results of the Schiavone *et al.* study[29] in Fig 8b. Since the stent geometrical design is same for both studies, we only applied the material properties of the PLLA that is reported in Schiavone *et al.* study.[29] The stent recoil with the new material properties (13.2%) is much higher than its value for the reference material (3.3%) and this difference indicates on the importance of obtaining precise values of material properties for stent analysis. The stent recoil after expansion in the Schiavone *et al.* study[29] is 17% and its difference with our result is due to the several reasons including lower expansion ratio and not considering the plastic deformation of plaque in Schiavone *et al* study.[29]

The initial and original radial strength of the Absorb BVS model is compared with the numerical and
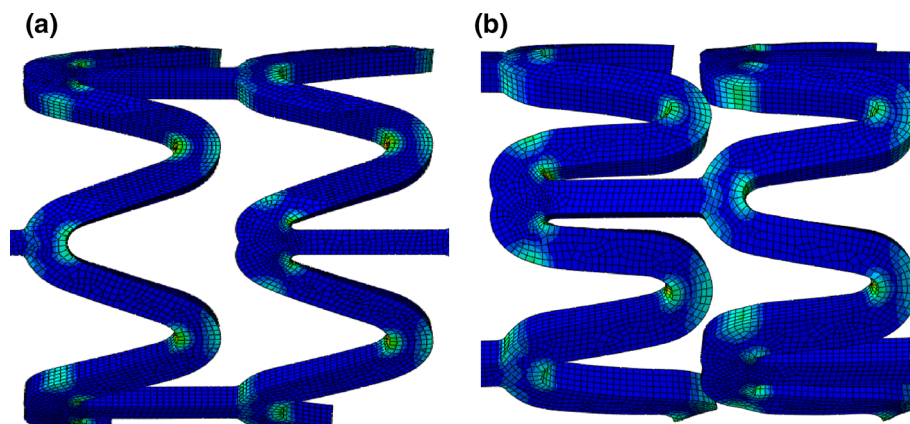

FIGURE 7. Deformation of Absorb BVS stent during crimping. (a) Simulation results at OD = 2.6 mm. (b) Simulation results at OD = 1.8 mm.
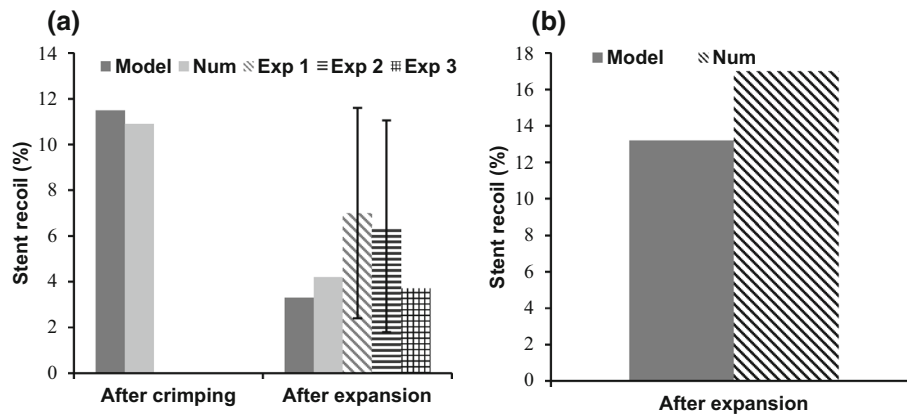
FIGURE 8. The comparison of stent recoil of the Absorb BVS stent with other numerical and experimental results. (a) Comparison of simulation results with reference material (Model) and the results of Wang et al.[39] (Num), Borgi et al.[3] (Exp 1), Verheye et al.[38] (Exp 2) and manufacturer data[35] (Exp 3). (b) Comparison of simulation results and results of Schiavone et al.[29] (Num) with same PLLA material properties.
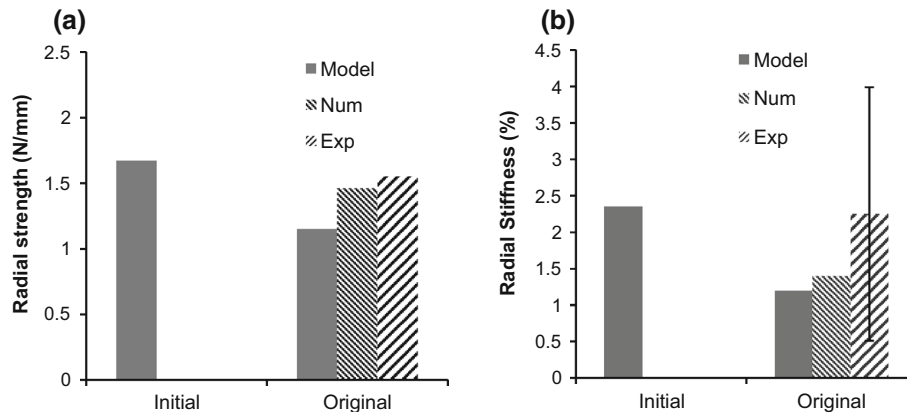

FIGURE 9. The comparison of radial strength and stiffness of the Absorb BVS stent with other numerical and experimental results. (a) Comparison of calculated radial strength (Model) and the results of Wang et al. study[39] (Num, Exp) (b) Comparison of calculated radial stiffness and results of Wang et al.[39] (Num) and Schmidt et al.[31] (Exp) studies.

experimental results of Wang et al. study[39] in Fig. 9a. Considering the different simulation conditions in the two studies, the small discrepancy observed is acceptable. To compare the radial stiffness, according to the approach used in in Wang et al. study,[39] we calculated the difference in stent outer diameter between zero and 0.2 bar pressure in the radial loading curve and then normalize it to zero compression diameter. The initial and original radial stiffness of the Absorb BVS stent in the model, the simulation results of Wang et al. study[39] and the experimental results of Schmidt et al. study[31] are compared in Fig. 9b. Schmidt et al.[31] in their study investigated the mechanical properties of nine different commercial stent designs and calculated the normalized radial stiffness of these stents. The results show that the obtained radial stiffness for the Absorb BVS stent in our model is in the range of the radial stiffness of the commercial stents examined by Schmidt et al.[31] and also our model reproduces the simulation results

of Wang et al. study[39] in terms of radial stiffness. The results also show that, despite the acceptability of the radial stiffness of the Absorb BVS stent, this stent has less radial stiffness compared to other metal stents. In three-point bending test, the bending stiffness of the Absorb BVS stent is obtained equal to 3.21 N mm² that is nearly close to the bending stiffness of the stent model in Wang et al. study[39] which is 4.01 N mm².

For the Xience Stent, by applying the material properties of the cobalt-chromium alloy L605,[30] the stenting process has been simulated and its functional characteristic were obtained. The stent recoil after expansion is compared with the experimental data in Fig. 10a. Also, the radial strength of Xience stent is compared with the radial strength of the Absorb BVS stent and the manufacturer data in Fig. 10b. According to the Fig. 10, the simulation results are in good agreement with experimental and manufacturer data. The low difference in the results is due to different test
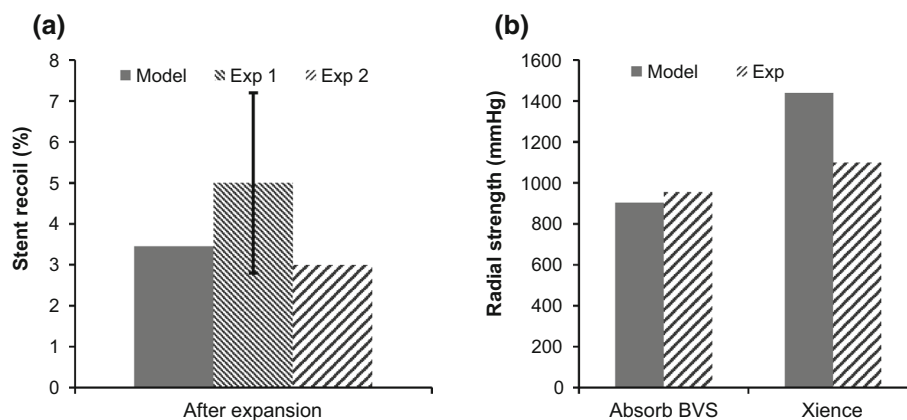
BMES BIOMEDICAL ENGINEERING SOCIETY

FIGURE 10. The comparison of Xience stent's simulated results with other numerical and experimental results. (a) Comparison of Xience stent recoil after expansion and the results of Schmidt et al. study[31] (Exp1) and manufacturer data[35] (Exp 2) (b) Comparison of calculated radial strength of both stents and manufacturer data[35] (Exp).

conditions and the lack of access to the exact values of the material properties in commercial stents. The results also show that both stents satisfy the required condition for the radial strength which should be more than 350 mmHg.[35]

Schiavone et al.[30] in their study on the Xience stent showed that using low-strength material results in the stent's larger recoil and wrongly interpreted this behavior is due to the low yield stress and weak strain-hardening of the material. But we showed that except of very low yield stresses, decrease in the yield or ultimate stress results in the decrease of stent recoil. In fact, they overlooked the major effect of the lower Young's modulus on the elevation of stent recoil. So, it is necessary for analyzing stent performance, to somehow fix other material properties except the examined one.

CONCLUSION

In this study, we examined two commercial stent designs to investigate the sensitivity of the stent functional characteristics to material plastic properties for artificial and existing commercial stent materials. We modeled Absorb BVS stent for low-strength materials, such as polymers, and Xience stent for high-strength materials such as metallic alloys. The results showed that increase in the yield stress resulted in the elevation of radial strength, radial stiffness, max crimping and expanding force of stent and reduction of arterial wall stress and strain and residual plastic strain of stent, and consequently enhanced the stent mechanical performance. On the other hand, increase in the yield stress elevated stent recoil and decreased stent flexibility and consequently diminished stent performance. The increase in the ultimate stress had a similar dual effect on the stent mechanical performance, but its

effect on both stents was usually lower. Except in some cases, the Absorb BVS and Xience stents had almost similar sensitivity to the variations in the material yield and ultimate stresses. Finally, the simulation results were validated against the experimental and numerical results of other studies.

ELECTRONIC SUPPLEMENTARY MATERIAL

The online version of this article (https://doi.org/10.1007/s13239-019-00450-1) contains supplementary material, which is available to authorized users.

ACKNOWLEDGMENTS

We convey our thanks to Dr. M. Dehghani and Dr. A. Alamdar for their great help.

CONFLICT OF INTEREST

Ali Khalilimeybodi, Amir Alishzadeh Khoei and Babak Sharif-Kashani declare that they have no conflict of interest.

ETHICAL APPROVAL

This article does not contain any studies with human participants or animals performed by any of the authors.

REFERENCES

[1]Azaouzi, M., A. Makradi, and S. Belouettar. Numerical investigations of the structural behavior of a balloon

expandable stent design using finite element method. *Comput. Mater. Sci.* 72:54–61, 2013.

[2]Bobel, A. C., S. Petisco, J. R. Sarasua, W. Wang, and P. E. McHugh. Computational bench testing to evaluate the short-term mechanical performance of a polymeric stent. *Cardiovasc. Eng. Technol.* 6(4):519–532, 2015.

[3]Borghi, T. C., J. R. Costa, A. Abizaid, D. Chamié, M. V. e Silva, D. Taiguara, R. Costa, R. Staico, F. Feres, Á. J. Chaves, and D. Siqueira. Comparison of acute stent recoil between the everolimus-eluting bioresorbable vascular scaffold and two different drug-eluting metallic stents. *Revista Brasileira de Cardiologia Invasiva (English Edition)* 21(4):326–331, 2013.

[4]Bowen, P. K., E. R. Shearier, S. Zhao, R. J. Guillory, F. Zhao, J. Goldman, and J. W. Drelich. Biodegradable metals for cardiovascular stents: from clinical concerns to recent Zn-Alloys. *Adv. Healthc. Mater.* 5(10):1121–1140, 2016.

[5]Chen, C., Y. Xiong, W. Jiang, Y. Wang, Z. Wang, and Y. Chen. Experimental and numerical simulation of biodegradable stents with different strut geometries. *Cardiovasc. Eng. Technol.* 2019. https://doi.org/10.1007/s13239-019-00433-2.

[6]De Beule, M., P. Mortier, S. G. Carlier, B. Verhegghe, R. Van Impe, and P. Verdonck. Realistic finite element-based stent design: the impact of balloon folding. *J. Biomech.* 41(2):383–389, 2008.

[7]Diez, M., M. H. Kang, S. M. Kim, H. E. Kim, and J. Song. Hydroxyapatite (HA)/poly-L-lactic acid (PLLA) dual coating on magnesium alloy under deformation for biomedical applications. *J. Mater. Sci.* 27(2):34, 2016.

[8]Drumright, R. E., P. R. Gruber, and D. E. Henton. Polylactic acid technology. *Adv. Mater.* 12(23):1841–1846, 2000.

[9]Everett, K. D. Mechanisms and implications of fracture in cardiovascular stents (Doctoral dissertation, Harvard University). 2014.

[10]Gervaso, F., C. Capelli, L. Petrini, S. Lattanzio, L. Di Virgilio, and F. Migliavacca. On the effects of different strategies in modelling balloon-expandable stenting by means of finite element method. *J. Biomech.* 41(6):1206–1212, 2008.

[11]Grogan, J. A., S. B. Leen, and P. E. McHugh. Comparing coronary stent material performance on a common geometric platform through simulated bench testing. *J. Mech. Behav. Biomed. Mater.* 12:129–138, 2012.

[12]Holzapfel, G. A., G. Sommer, C. T. Gasser, and P. Regitnig. Determination of layer-specific mechanical properties of human coronary arteries with nonatherosclerotic intimal thickening and related constitutive modeling. *Am. J. Physiol. Heart Circ. Physiol.* 289(5):H2048–H2058, 2005.

[13]Idziak-Jabłońska, A. Stress and strain distribution in expanded coronary stents depending on applied material. *J. Appl. Math. Comput. Mech.* 14(2):21–30, 2015.

[14]Imani, M., A. M. Goudarzi, D. D. Ganji, and A. L. Aghili. The comprehensive finite element model for stenting: The influence of stent design on the outcome after coronary stent placement. *J. Theor. Appl. Mech.* 51(3):639–648, 2013.

[15]Lally, C., F. Dolan, and P. J. Prendergast. Cardiovascular stent design and vessel stresses: a finite element analysis. *J. Biomech.* 38(8):1574–1581, 2005.

[16]Lee, S. Continuum deformation model for drug-eluting stent (DES) medical devices using finite element analysis

(FEA) (Doctoral dissertation, The University of Wisconsin-Milwaukee). 2013.

[17]Loree, H. M., A. J. Grodzinsky, S. Y. Park, L. J. Gibson, and R. T. Lee. Static circumferential tangential modulus of human atherosclerotic tissue. *J. Biomech.* 27(2):195–204, 1994.

[18]Martin, D., and F. J. Boyle. Computational structural modelling of coronary stent deployment: a review. *Comput. Methods Biomech. Biomed. Eng.* 14(04):331–348, 2011.

[19]Moore, J. E., J. S. Soares, and K. R. Rajagopal. Biodegradable stents: biomechanical modeling challenges and opportunities. *Cardiovasc. Eng. Technol.* 1(1):52–65, 2010.

[20]Morlacchi, S., G. Pennati, L. Petrini, G. Dubini, and F. Migliavacca. Influence of plaque calcifications on coronary stent fracture: a numerical fatigue life analysis including cardiac wall movement. *J. Biomech.* 47(4):899–907, 2014.

[21]Obayi, C. S., R. Tolouei, A. Mostavan, C. Paternoster, S. Turgeon, B. A. Okorie, D. O. Obikwelu, and D. Mantovani. Effect of grain sizes on mechanical properties and biodegradation behavior of pure iron for cardiovascular stent application. *Biomatter.* 6(1):e959874, 2016.

[22]Parker, T., V. Dave, and R. Falotico. Polymers for drug eluting stents. *Curr. Pharm. Des.* 16(36):3978–3988, 2010.

[23]Pauck, R. G., and B. D. Reddy. Computational analysis of the radial mechanical performance of PLLA coronary artery stents. *Med. Eng. Phys.* 37(1):7–12, 2015.

[24]Pericevic, I., C. Lally, D. Toner, and D. J. Kelly. The influence of plaque composition on underlying arterial wall stress during stent expansion: the case for lesion-specific stents. *Med. Eng. Phys.* 31(4):428–433, 2009.

[25]Poncin, P., Millet, C., Chevy, J., Proft, J. L. Comparing and optimizing Co–Cr tubing for stent applications. Proceedings of the materials and processes for medical devices conference, 2004 (pp. 279–283).

[26]Qiu, T. Y., M. Song, and L. G. Zhao. A computational study of crimping and expansion of bioresorbable polymeric stents. *Mech. time-Depend. Mater.* 22(2):273–290, 2018.

[27]Qiu, T. Y., L. G. Zhao, and M. Song. A computational study of mechanical performance of bioresorbable polymeric stents with design variations. *Cardiovasc. Eng. Technol.* 10(1):46–60, 2019.

[28]Sarasua, J. R., A. L. Arraiza, P. Balerdi, and I. Maiza. Crystallinity and mechanical properties of optically pure polylactides and their blends. *Polym. Eng. Sci.* 45(5):745–753, 2005.

[29]Schiavone, A., C. Abunassar, S. Hossainy, and L. G. Zhao. Computational analysis of mechanical stress–strain interaction of a bioresorbable scaffold with blood vessel. *J. Biomech.* 49(13):2677–2683, 2016.

[30]Schiavone, A., L. G. Zhao, and A. A. Abdel-Wahab. Effects of material, coating, design and plaque composition on stent deployment inside a stenotic artery—finite element simulation. *Mater. Sci. Eng. C* 42:479–488, 2014.

[31]Schmidt, W., P. Behrens, and K. P. Schmitz. Biomechanical Aspects of Potential Stent Malapposition at Coronary Stent Implantation. In World Congress on Medical Physics and Biomedical Engineering, Munich, Germany. Berlin: Springer, pp. 136–139, 2009.

[32]Standard A F2606-08. Standard guide for three-point bending of balloon expandable vascular stents and stent systems. ASTM International, West Conshohocken. 2014; https://doi.org/10.1520/f2606.

[33] Standard A F3067-14. Guide for radial loading of balloon expandable and self expanding vascular stents. ASTM International, West Conshohocken. 2014; https://doi.org/10.1520/F3067-14.

[34] Takashima, K., T. Kitou, K. Mori, and K. Ikeuchi. Simulation and experimental observation of contact conditions between stents and artery models. *Med. Eng. Phys.* 29(3):326–335, 2007.

[35] U.S. Food and Drug Administration tcsdpac. Absorb Gt1^TM Bioresorbable Vascular Scaffold System. 2016.

[36] Uurto, I., A. Kotsar, T. Isotalo, J. Mikkonen, P. M. Martikainen, M. Kellomäki, P. Törmälä, T. L. Tammela, M. Talja, and J. P. Salenius. Tissue biocompatibility of new biodegradable drug-eluting stent materials. *J. Mater. Sci.* 18(8):1543–1547, 2007.

[37] Vaizasatya, A. A methodology for coronary stent product development: design, simulation and optimization. Doctoral dissertation, North Carolina Agricultural and Technical State University. 2013.

[38] Verheye, S., J. A. Ormiston, J. Stewart, M. Webster, E. Sanidas, R. Costa, J. R. Costa, D. Chamie, A. S. Abizaid, I. Pinto, and L. Morrison. A next-generation bioresorbable coronary scaffold system: from bench to first clinical evaluation: 6-and 12-month clinical and multimodality imaging results. *JACC* 7(1):89–99, 2014.

[39] Wang, Q., G. Fang, Y. Zhao, G. Wang, and T. Cai. Computational and experimental investigation into mechanical performances of Poly-L-Lactide Acid (PLLA) coronary stents. *J. Mech. Behav. Biomed. Mater.* 65:415–427, 2017.

[40] Wu, W., D. Gastaldi, K. Yang, L. Tan, L. Petrini, and F. Migliavacca. Finite element analyses for design evaluation of biodegradable magnesium alloy stents in arterial vessels. *Mater. Sci. Eng. B* 176(20):1733–1740, 2011.

[41] Wu, W., W. Q. Wang, D. Z. Yang, and M. Qi. Stent expansion in curved vessel and their interactions: a finite element analysis. *J. Biomech.* 40(11):2580–2585, 2007.

[42] Yang, H. Study of mechanical performance of stent implants using theoretical and numerical approach. Doctoral dissertation, University of North Texas. 2015.

[43] Yu, C., and J. Kohn. Tyrosine–PEG-derived poly (ether carbonate) s as new biomaterials: part I: synthesis and evaluation. *Biomaterials* 20(3):253–264, 1999.

[44] Yun, Y., Z. Dong, N. Lee, Y. Liu, D. Xue, X. Guo, J. Kuhlmann, A. Doepke, H. B. Halsall, W. Heineman, and S. Sundaramurthy. Revolutionizing biodegradable metals. *Mater. Today* 12(10):22–32, 2009.

[45] Zhao S. Biomechanical response of artery following stent implantation: Implication for restenosis. Doctoral dissertation, University of Nebraska. 2013.